HHS Public Access

Author manuscript

Adv Mater. Author manuscript; available in PMC 2023 August 01.

Published in final edited form as:

Adv Mater. 2022 August ; 34(34): e2200656. doi:10.1002/adma.202200656.

Tunable Strong Coupling in Transition Metal Dichalcogenide Nanowires

Jingang Li,

Kan Yao,

Yun Huang,

Jie Fang,

Pavana Siddhartha Kollipara,

Donglei Emma Fan,

Yuebing Zheng

Walker Department of Mechanical Engineering, Materials Science & Engineering Program and Texas Materials Institute, University of Texas at Austin, Austin, TX 78712, USA.

Abstract

Subwavelength optical resonators with spatiotemporal control of light are essential to the miniaturization of optical devices. In this work, chemically synthesized transition metal dichalcogenide (TMDC) nanowires are exploited as a new type of dielectric nanoresonators to simultaneously support pronounced excitonic and Mie resonances. Strong light-matter couplings and tunable exciton polaritons in individual nanowires are demonstrated. In addition, the excitonic responses can be reversibly modulated with excellent reproducibility, offering the potential for developing tunable optical nanodevices. Being in the mobile colloidal state with highly tunable optical properties, the TMDC nanoresonators will find promising applications in integrated active optical devices, including all-optical switches and sensors.

Graphical Abstract

dfan@austin.utexas.edu (D.F.), zheng@austin.utexas.edu (Y.Z.).

Conflict of Interest

The authors declare no conflict of interest.

Supporting Information

Supporting Information is available from the Wiley Online Library or from the author.

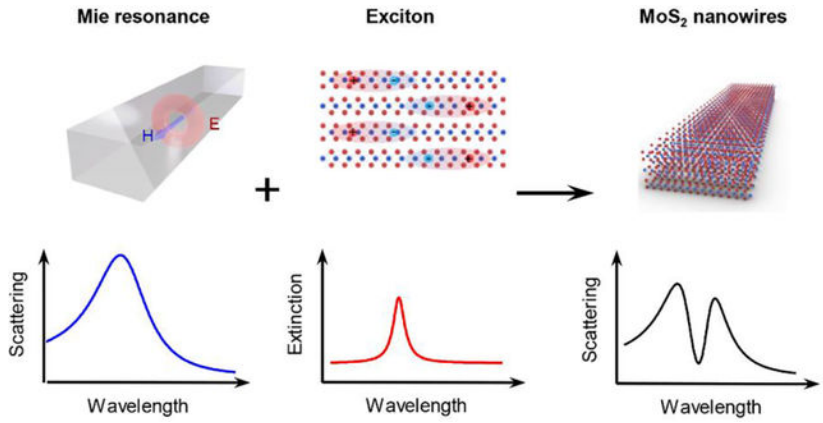

Chemically synthesized transition metal dichalcogenide (TMDC) nanowires are exploited as a new type of subwavelength optical nanoresonators to simultaneously support pronounced excitonic and Mie resonances. Strong coupling between excitons and Mie resonances is demonstrated to support Mie-exciton polaritons. Moreover, the optical coupling can be further tuned by optothermal effects in a reversible and reproducible way.

Keywords

nanowires; transition metal dichalcogenides; strong coupling; exciton polaritons; thermo-optic tunability

1. Introduction

Transition metal dichalcogenides (TMDCs) are an emerging class of materials with extraordinary physical properties,[1] including excitonic effects,[2] tunable bandgaps,[3] and valley polarization.[4] In particular, TMDC monolayers have attracted significant research attention due to their direct bandgaps at the visible and near-infrared wavelengths.[5, 6] These properties make TMDCs attractive for a wide range of electronic, photonic, and optoelectronic applications,[7, 8] such as transistor,[9, 10] photodetection,[11, 12] light-emission,[13] and lasing.[14] In addition, strong light-matter interactions between TMDCs and optical cavities, resonant plasmonic or dielectric structures have been demonstrated,[15–18] resulting in the formation of exciton polaritons with rich physics for quantum optics and polaritonic devices.[19, 20]

While TMDCs have been extensively explored as an excitonic platform with novel optical and electronic functionalities, it is less appreciated that TMDCs also have a high refractive index.[21] Compared to the widely investigated plasmonic systems, high-index dielectric materials show low loss at visible frequencies, pronounced electric and magnetic optical resonances, and high compatibility with complementary metal-oxide-semiconductor fabrication.[22, 23] Dielectric metamaterials based on silicon have rapidly emerged as a popular platform for a wealth of applications in integrated electronics and photonics.[24] Recently, multilayer TMDC nanostructures have been studied as high-index nanoresonators with strong Mie resonances.[25, 26] The presence of excitons in TMDCs further enables the

formation of unique self-hybridized exciton polaritons,[26, 27] which remarkably enrich the capabilities of nanophotonic systems. Additionally, nanostructured TMDC photonic crystals and gratings have been demonstrated with enhanced control of light for advanced photonic applications.[28, 29]

Here, we report strong coupling between excitons and Mie resonances in individual TMDC nanowires. Molybdenum disulfide (MoS_2) nanowires are chemically synthesized with tailorable dimensions to support tunable Mie-exciton polaritons in visible wavelengths. Compared to previously reported TMDC nanoresonators that are fabricated by lithographical methods (e.g., electron beam lithography),[25, 26] colloidal MoS_2 nanowires provide additional possibilities in the design and fabrication of nanophotonic devices. Specifically, the chemical synthesis approach permits the scalable and high-throughput production of TMDC nanoresonators with tunable dimensions, which can be easily integrated with other techniques for on-demand dispersion, transfer, manipulation, and assembly. Moreover, we show that the MoS_2 excitonic properties and spectral splittings can be optothermally modulated under laser illumination, which offers a promising platform for the development of tunable photonic systems.

2. Results and Discussion

MoS_2 nanowires were synthesized from MoO_3 nanowire precursors via a two-step sulfurization process (see Experimental Section).[30] The first sulfurization reaction at 500 °C converted MoO_3 nanowires to more thermally stable MoS_2/MoO_2 hybrid nanowires, after which a second sulfurization process was carried out at 900 °C to produce pure MoS_2 nanowires (Figure 1a and Note S1). Scanning electron microscope (SEM), high-resolution transmission electron microscope (TEM), and selected area electron diffraction (SAED) were used for materials characterization. The synthesized MoS_2 nanowires have a typical length of 5–20 μm (Figure 1b,c). The symmetrical hexagonal diffraction patterns indicated a hexagonal lattice structure (Figure 1d), and the sharp atomic images also showed a high crystalline quality (Figure 1e). In addition, the corresponding X-ray diffraction (XRD) and Raman spectra further confirmed the crystal structure and chemical purity of MoS_2 nanowires (Figure 1f,g). It should be noted that MoO_3 nanowires serve as both the precursor and the fabrication template, which enables the synthesis of MoS_2 nanowires with controllable dimensions by simply tuning the dimensions of MoO_3 nanowires. In this study, the thickness of MoS_2 nanowires is controlled at ~ 65 nm (Figure S1), while the width is varied to modulate the optical responses.

The optical responses of MoS_2 nanowires are illustrated in Figure 2a–c. In addition to intrinsic exciton resonances (Figure 2b), the high refractive index of MoS_2 gives rise to pronounced Mie resonances (Figure 2a). The strong coupling between exciton and Mie resonances leads to the peak splitting in the scattering spectra (Figure 2c). Leaky/guided modes are also allowed in dielectric nanowires, which nonetheless cannot be excited efficiently with plane waves unless using near grazing incidence.[31] We measured optical scattering from individual MoS_2 nanowires with a varying width using dark-field spectroscopy (see Experimental Section) and correlated the spectra with the morphologies of nanowires via SEM imaging (Figure 2f). Figure 2d,e shows the experimental dark-field

scattering spectra and the corresponding full-wave simulations for three MoS_2 nanowires with a thickness of 65 nm and a width of 100, 160, and 200 nm (see Experimental Section). Considering the anisotropic morphology of nanowires, we studied the scattering responses under both transverse-electric (TE, Figure 2d) and transverse-magnetic (TM, Figure 2e) illumination, where the incident light was linearly polarized with the electric field either perpendicular (TE) or parallel (TM) to the nanowire axis.

The experimental and simulated spectra of MoS_2 nanowires are in good agreement for both polarizations. The most notable features of all scattering spectra are two dips at ~ 665 nm and ~ 612 nm, corresponding to the A and B excitons of MoS_2, respectively. The dips arise from the coupling between the excitons and Mie resonance, which leads to the formation of three Mie-exciton hybrid modes. Strong coupling is evidenced by dips at the same wavelengths in the absorption spectra (Figure S2).[32] We also confirmed that the spectral dips still remain at the same positions with the varying thickness of nanowires (Figure S3). In addition, the whole scattering profile shows a gradual redshift with the increasing width of MoS_2 nanowires, which is consistent with the size-dependent behavior of Mie resonances. The scattering spectra under TE and TM excitation exhibit peaks in similar positions, while the peak at the longer wavelength is stronger under TM polarization. This quantitative difference can be attributed to the two-fold degeneracy of a higher-order mode compared to the non-degenerate TE01 mode (i.e., the magnetic dipole in this case), which can be seen in the Mie formulas for infinite cylinders[31] and is consistent with the previously reported observations.[33]

Figure 3a plots the experimental scattering map for MoS_2 nanowires with a varying width from 100 to 240 nm under TE-polarized excitation. The green dot lines highlight the three polariton branches, and the grey dot lines mark two fixed dips at exciton resonances. The simulated map agrees well with the experimental results (Figure 3b), where all excitonic and polaritonic features are reproduced. Similar results were also obtained under TM-polarized excitation (Figure S4). Figure 3c shows the field distributions at the wavelength of 640 nm between A and B excitons for TE polarization, where a dominant magnetic dipole resonance is clearly recognized. To gain deeper understanding of the interactions between excitons and Mie resonances, we conducted multipole decomposition by retrieving the multipole moments of the nanowires from simulated field distributions. For an infinite nanowire aligned along the z-axis, the Mie coefficients can be expressed by

$$a_m = -\frac{\eta k}{4}\int \mathbf{J}_z e^{im\varphi} J_m(kr) d\mathrm{s} \tag{1}$$

for TM polarization and

$$b_m = \frac{i}{4}\int \frac{e^{im\varphi}}{r}\left[kr\mathbf{J}_\varphi J_{m+1}(kr) + m\left(i\mathbf{J}_r - \mathbf{J}_\varphi\right)J_m(kr)\right] d\mathrm{s} \tag{2}$$

for TE polarization.[34] Here, m takes integers, r and φ are the polar coordinates, η is the wave impedance of the host medium, k is the wave number, $J_m(\cdot)$ is the Bessel function of the first kind and order m, $\mathbf{J} = -i\omega\varepsilon_0(\varepsilon - \varepsilon_h)\mathbf{E}$ is the current induced by the total electric field

E with ε and ε_h the relative permittivities of the nanowire and host medium, respectively. The scattering cross section of the nanowire C_s can be calculated from these coefficients by

$$C_s = \frac{4}{kE_0^2}\sum_{m=-\infty}^{m=\infty}(|a_m|^2 + \eta^2|b_m|^2) \tag{3}$$

where E_0 is the amplitude of the electric field of the incident plane wave. Figure 3d shows the simulated scattering cross section of a nanowire for TE polarization, along with the contributions from individual Mie resonances. Scattering is dominated by only three terms ($m = 0, \pm 1$), of which the positive and negative orders are degenerate due to symmetry. Noticeably, excitons are predominantly coupled to the magnetic dipole resonance (b_0), as can be concluded by comparing the decomposed contributions to the scattering spectrum in Figure 3e, where the A and B excitons are artificially turned off in the dielectric function (see Experimental Section and Figure S5). Interestingly, the coupling to electric dipole (a_0) and magnetic dipole ($a_{\pm 1}$) resonances is comparable for TM polarization (Figure S6). We attribute the dominance of coupling to magnetic dipole mode under TE-polarized excitation to the characteristic mode profiles. When the incident field is polarized parallel to the cross-sectional plane, the formation of a magnetic dipole mode requires strong circulating electric fields inside the nanowire (Figure 3c), whereas the interior electric fields of an electric dipole mode are less intense as a consequence of the high refractive index and continuity requirement of the electric displacement. For TM polarization, this difference between electric and magnetic modes is not significant, and the interior electric fields are polarized in the unbounded direction along the nanowire axis. Thus, a more sophisticated model is needed to consider the simultaneous involvement of electric and magnetic modes, which is beyond this work.

The fact that only the magnetic dipole resonance is active in coupling under TE polarization allows us to investigate the coupled system with additional Hamiltonian analysis (see Note S2 for more details). The Hamiltonian matrix of the coupled system can be written as[35]

$$\widehat{\mathscr{H}} = \hbar\begin{pmatrix} \omega_{\mathrm{MD}} - i\frac{\gamma_{\mathrm{MD}}}{2} & g_{\mathrm{A}} & g_{\mathrm{B}} \\ g_{\mathrm{A}} & \omega_{\mathrm{A}} - i\frac{\gamma_{\mathrm{A}}}{2} & 0 \\ g_{\mathrm{B}} & 0 & \omega_{\mathrm{B}} - i\frac{\gamma_{\mathrm{B}}}{2} \end{pmatrix}, \tag{4}$$

where ω_{MD} (γ_{MD}), ω_{A} (γ_{A}), and ω_{B} (γ_{B}) are the frequencies (linewidths, i.e., full width at half maximum) of the magnetic dipole resonance, A exciton, and B exciton, respectively; and $g_{\mathrm{A/B}}$ represents the coupling strength between A/B exciton and the magnetic dipole resonance. The parameters used to solve the polariton eigenfrequencies are summarized in Table 1. Figure 3f shows the anticrossing behaviors of three polariton branches in MoS_2 nanowire under room temperature (also see Figure S7 for the experimental spectra). The extracted Rabi splitting between the upper and lower polariton branches $\Omega_{\mathrm{UP\text{-}LP}}$ is ~ 450 meV, which fulfils the criteria of strong coupling $\Omega_{\mathrm{UP\text{-}LP}} > \gamma_{\mathrm{MD}}$. In addition, the Rabi splittings between the upper and middle polariton ($\Omega_{\mathrm{UP\text{-}MP}}$) and middle and lower polariton

($\Omega_{MP\text{-}LP}$) can be extracted at the zero detuning between magnetic dipole mode and B exciton and magnetic dipole mode and A exciton, respectively, as $\Omega_{UP\text{-}MP} \sim 243$ meV and $\Omega_{MP\text{-}LP} \sim 262$ meV. Both meet the strong coupling condition as $\Omega_{UP\text{-}MP} > (\gamma_{MD} + \gamma_B)/2$ and $\Omega_{MP\text{-}LP} > (\gamma_{MD} + \gamma_A)$. We further fitted the measured scattering spectra via coupled-mode theory (CMT, see Note S3 for more details).[36, 37] The CMT fitting results are in good agreement with the experimental spectra (Figure S8) and the fitting parameters are consistent with the Hamilton analysis (Table S1). From the CMT fitting results, the coupling strength $g_{A/B}$ fulfills the criteria of strong coupling,[37, 38] $g_{A/B} > \sqrt{\frac{\gamma_{MD}^2 + \gamma_{A/B}^2}{8}}$, which further confirmed the strong coupling regime. It should be noted that the coupling strength g is proportional to $\sqrt{N}$, where N is the number of excitons in the coupling region.[35] In our case, strong coupling is guaranteed with the effective spectral and spatial overlaps between Mie resonances and the large quantity of excitons in MoS_2 nanowires.

The capability of tuning excitonic properties and scattering responses is appealing for applications in photonic devices. Previously, exciton tuning has been demonstrated in TMDCs through ionic-liquid gating.[39] In this work, due to the high optical absorption of MoS_2 nanowires (Figure S9),[40] the MoS_2 excitonic properties can be optothermally modulated by light illumination. Under low-power laser irradiation, the exciton dips in the scattering spectra gradually redshifted and became suppressed along with the increasing optical power (Figure 4a). The spectral splittings became not observable at a laser power of 1.1 mW. To further understand this tuning behavior, we extracted the temperature-dependent excitonic energy and linewidth from the CMT fitting (Figure S10 and Table S2). The energy redshift and linewidth broadening can be clearly observed for both A and B excitons (Figure 4b and Figure S11). The excitonic energy as a function of temperature can be described by the O'Donnell model:[41]

$$E_{A/B}(T) = E_{A/B}(0) - S\langle\hbar\omega\rangle[\coth(\frac{\langle\hbar\omega\rangle}{2k_BT}) - 1] \quad (5)$$

where $E_{A/B}(T)$ and $E_{A/B}(0)$ are the energy of A/B excitons at the temperature of T and 0 K, respectively, S is a dimensionless coupling constant to phonons, $\langle\hbar\omega\rangle$ is the average phonon energy, and k_B is the Boltzmann constant. And the excitonic linewidth broadening can be modeled by[42]

$$\gamma_{A/B}(T) = \gamma_{A/B}(0) - \gamma' T \quad (6)$$

where $\gamma_{A/B}(T)$ and $\gamma_{A/B}(0)$ are the linewidth of A/B excitons at the temperature of T and 0 K, respectively, γ' is the exciton-phonon coupling strength. The extracted temperature-dependent excitonic energy and linewidth were well fitted by the theoretical models in Equation (5) and (6) (Figure 4b and Figure S11), indicating that the obtained temperature-dependent excitonic features are reliable. In addition, we noted that the coupling strength in the system slightly decreased along with the temperature rise (Table S3), which is likely resulted from the lower exciton population coupled to the Mie resonance at high temperatures.[43] Furthermore, this optical exciton tuning in MoS_2 nanowires is estimated to happen at a timescale of several nanoseconds[44] in a fully reversible and highly repeatable

way (Figure 4c), highlighting their potential applications in light modulation and tunable optical devices.

3. Conclusion

In summary, we report MoS_2 nanowires as subwavelength resonators that support strong light-matter coupling and Mie-exciton polaritons at room temperature. The TMDC nanoresonators present a new class of dielectric materials for integrated photonics systems, such as waveguides, metamaterials, and optical modulators.[21] With the existence of Mie resonances and excitonic responses, they also provide a promising platform to be coupled to other active materials, such as quantum dots and monolayer TMDCs, to tailor their linear and/or nonlinear emission.[45–47] The MoS_2 excitonic properties can be further tuned due to the strong light-to-heat conversion, leading to all-optical modulation of scattering responses at the exciton wavelengths. This reversible and reproducible thermo-optic modulation makes MoS_2 nanowires promising as tunable optical components in integrated photonics, such as all-optical switch,[44] optical nanoantennas,[48] and metalenses.[49] In addition, the colloidal state of MoS_2 nanowires presented here offers extra flexibility for their implementation in photonic devices. For example, the easy integration of optical manipulation[50, 51] and electric manipulation[30, 52, 53] techniques permits the controlled trapping, positioning, and assembly of multiple nanowires to more complex superstructures for enhanced functionalities.

4. Experimental Section

Synthesis of MoS_2 nanowires.

First, MoO_3 nanowires were synthesized as the precursor via a facile hydrothermal method. In a typical synthesis, 1 g ammonium heptamolybdate tetrahydrate ($(NH_4)_6Mo_7O_{24}$ $4H_2O$) was dissolved into 20 mL deionized (DI) water under vigorous stirring, followed by the addition of 5 mL HNO_3. The as-prepared solution was then transferred to a 30 ml Teflon autoclave and heated at 180 °C for 20 hours. After cooling, white precipitates were collected, washed, centrifuged, and dried overnight to obtain the powder of MoO_3 nanowires. Next, MoS_2/MoO_2 hybrid nanowires were synthesized by a chemical vapor deposition method in a vacuum tube furnace. In a typical process, two quartz boats filled with 0.1 g as-synthesized MoO_3 nanowires and 0.5 g sulfur powder, respectively, were inserted into a one-end-sealed quartz tube with a 20 cm distance. Ar gas (50 sccm) was used as the carrier gas. The tube pressure was reduced to 20 mTorr, and the heating temperature was set as 500 °C. At this temperature, sulfur vapor was carried downstream to react with MoO_3 nanowires for about 30 mins, after which the white MoO_3 powder turned black as MoS_2/MoO_2 nanowires powder. Last, pure MoS_2 nanowires were synthesized by a further sulfurization of the as-obtained MoS_2/MoO_2 powder for 30 mins. A similar setup as mentioned above was used, except the temperature was set at 900 °C, and the Ar gas flow was set at 50 sccm.

Structural and compositional characterizations.

The morphology and crystal structure of MoS_2 nanowires were characterized using a Hitachi S-5500 SEM and a JEOL 2010 TEM. The composition of MoS_2 nanowires was characterized by Raman (Alpha 300, excited by 475 nm laser) and XRD (Rigaku MiniFlex 600).

Dark-field optical spectroscopy.

An inverted microscope (Nikon TiE) equipped with a 100× oil objective (Nikon, NA 0.5–1.3) was used. An oil-immersion dark-field condenser with a NA of 1.20–1.43 was used to focus the white illuminating light onto the MoS_2 nanowire from the top. A linear polarizer (Thorlabs) was used to filter unpolarized white light into linearly polarized light. The forward scattering signal from the MoS_2 nanowire was directed to an optical spectrometer (Andor) with a 500 nm grating. Background spectra were also recorded and subtracted to obtain the scattering signal of the MoS_2 nanowires. The scattering spectra were finally normalized by the incident light. In the optical exciton tuning experiments, a 532 nm laser (Coherent, Genesis MX STM-1 W) was directed to the microscope to heat the MoS_2 nanowire. A notch filter (NF 533–17, Thorlabs) was used to block the laser signal from entering the spectrometer.

COMSOL simulations.

We describe the dielectric function of MoS_2 using the Lorentz oscillator model. Three oscillators are included in the expression to account for the ground state transitions of A, B, and C excitons, respectively:

$$\varepsilon = \varepsilon_b + \sum_{j=1}^{3} f_i \frac{\omega_{ex,j}^2}{\omega_{ex,j}^2 - \omega^2 - i\gamma_{ex,j}\omega}, \quad (7)$$

where $\varepsilon_b = 13.7$ is the background permittivity from higher energy transitions, f_j, $\omega_{ex,j}$, and $\gamma_{ex,j}$ are the oscillator strengths, exciton energies, and exciton full widths of the three oscillators. All these ten parameters are determined by fitting, leading to reasonable agreement in line shape with the data from experiments, whereas better fits are viable if additional excited states of the excitons are included in the model.[54] In our current model, $f_1 = 0.7$, $\omega_{ex,1} = 1.84$ eV, and $\gamma_{ex,1} = 0.12$ eV for A exciton, $f_2 = 0.75$, $\omega_{ex,2} = 2.03$ eV, and $\gamma_{ex,16} = 0.16$ eV for B exciton, and $f_3 = 6.5$, $\omega_{ex,3} = 2.72$ eV, and $\gamma_{ex,3} = 0.57$ eV for C exciton, respectively (Figure S5a). The scattering and absorption properties of MoS_2 nanowires were simulated using the wave optics module of COMSOL Multiphysics 5.4. Because the lengths of the nanowires are much greater than the wavelengths of light, the nanowires were simply modeled on the cross-sectional plane as rectangles. To account for the real morphology from chemical synthesis, we rounded all the corners with a radius of 30 nm unless specified otherwise. The corner roundedness only slightly affects the magnitude of the simulated results with negligible effects on the spectral features (Figure S12). The dielectric function of the MoS_2 nanowires was assumed to be the same as those in the bulky state.[55] For calculation of the forward scattering signal as collected in the experiments, the differential power flow was integrated in the forward direction over an arc that spans the angle corresponding to the numerical aperture of the objective. Laser-induced heating

of MoS_2 nanowires is simulated using the heat transfer module. The system is modelled as a filleted block with dimensions 5 μm x 160 nm x 65 nm, with a fillet of 10 nm on all edges placed on a glass substrate. The heat capacity and thermal conductivity of MoS_2 NWs are functions of temperature.[56] The glass substrate has a heat capacity of 730 J kg^{-1} K^{-1} and thermal conductivity of 1.4 W m^{-1} K^{-1}. The heat source for the MoS_2 nanowire is modelled as a Gaussian profile with a beam radius of 500 nm and laser-beam power of 0.2–1.2 mW. The absorption at the laser wavelength (532 nm) is determined by using the method in ref.[57]. The heat flux through the MoS_2 nanowire surface boundaries and the top glass surface is set as convection with a net heat transfer coefficient of 10 W m^{-2} K^{-1} and a room temperature of 20 °C. All other glass domain boundaries (away from the MoS_2 nanowire) are set to be at room temperature.

Statistical Analysis.

Scattering spectra are normalized to [0, 1] before plotting the scattering map. The CMT fittings were performed using MagicPlot with the equations manually written into the software. The software used iterative Levenberg-Marquardt nonlinear least squares curve fitting algorithm to find the minimum residual sum of squares.

Supplementary Material

Refer to Web version on PubMed Central for supplementary material.

Acknowledgments

J.L., K.Y. and Y.H. contributed equally to this work. Y.Z., J.L., K.Y., J.F., and P.S.K. acknowledge the financial supports of the National Institute of General Medical Sciences of the National Institutes of Health (DP2GM128446) and the National Science Foundation (NSF-ECCS-2001650). D. F. and Y. H. would like to thank the support from Welch Foundation (F-1734), National Science Foundation (CMMI-1563382 and EECS-1710922, EECS-1930649 in part).

References

[1]. Manzeli S, Ovchinnikov D, Pasquier D, Yazyev OV, Kis A, Nat. Rev. Mater 2017, 2, 17033.

[2]. Novoselov KS, Mishchenko A, Carvalho A, Neto AHC, Science 2016, 353, aac9439. [PubMed: 27471306]

[3]. Xia F, Wang H, Xiao D, Dubey M, Ramasubramaniam A, Nat. Photonics 2014, 8, 899.

[4]. Mak KF, Xiao D, Shan J, Nat. Photonics 2018, 12, 451.

[5]. Mak KF, Lee C, Hone J, Shan J, Heinz TF, Phys. Rev. Lett 2010, 105, 136805. [PubMed: 21230799]

[6]. Splendiani A, Sun L, Zhang Y, Li T, Kim J, Chim C-Y, Galli G, Wang F, Nano Lett 2010, 10, 1271. [PubMed: 20229981]

[7]. Wang QH, Kalantar-Zadeh K, Kis A, Coleman JN, Strano MS, Nat. Nanotechnol 2012, 7, 699. [PubMed: 23132225]

[8]. Mak KF, Shan J, Nat. Photonics 2016, 10, 216.

[9]. Radisavljevic B, Radenovic A, Brivio J, Giacometti V, Kis A, Nat. Nanotechnol 2011, 6, 147. [PubMed: 21278752]

[10]. Kim S, Konar A, Hwang W-S, Lee JH, Lee J, Yang J, Jung C, Kim H, Yoo J-B, Choi J-Y, Jin YW, Lee SY, Jena D, Choi W, Kim K, Nat. Commun 2012, 3, 1011. [PubMed: 22910357]

[11]. Koppens FHL, Mueller T, Avouris P, Ferrari AC, Vitiello MS, Polini M, Nat. Nanotechnol 2014, 9, 780. [PubMed: 25286273]

[12]. Lopez-Sanchez O, Lembke D, Kayci M, Radenovic A, Kis A, Nat. Nanotechnol 2013, 8, 497. [PubMed: 23748194]

[13]. Pu J, Takenobu T, Adv. Mater 2018, 30, 1707627.

[14]. Wu S, Buckley S, Schaibley JR, Feng L, Yan J, Mandrus DG, Hatami F, Yao W, Vučković J, Majumdar A, Xu X, Nature 2015, 520, 69. [PubMed: 25778703]

[15]. Liu X, Galfsky T, Sun Z, Xia F, Lin E.-c., Lee Y-H, Kéna-Cohen S, Menon VM, Nat. Photonics 2015, 9, 30.

[16]. Liu W, Lee B, Naylor CH, Ee H-S, Park J, Johnson ATC, Agarwal R, Nano Lett 2016, 16, 1262. [PubMed: 26784532]

[17]. Lepeshov S, Wang M, Krasnok A, Kotov O, Zhang T, Liu H, Jiang T, Korgel B, Terrones M, Zheng Y, Alu A, ACS Appl. Mater. Interfaces 2018, 10, 16690. [PubMed: 29651843]

[18]. Kumar P, Lynch J, Song B, Ling H, Barrera F, Kisslinger K, Zhang H, Anantharaman SB, Digani J, Zhu H, Choudhury TH, McAleese C, Wang X, Conran BR, Whear O, Motala MJ, Snure M, Muratore C, Redwing JM, Glavin NR, Stach EA, Davoyan AR, Jariwala D, Nat. Nanotechnol 2021.

[19]. Basov DN, Fogler MM, García de Abajo FJ, Science 2016, 354, aag1992. [PubMed: 27738142]

[20]. Hu F, Luan Y, Scott ME, Yan J, Mandrus DG, Xu X, Fei Z, Nat. Photonics 2017, 11, 356.

[21]. Ling H, Li R, Davoyan AR, ACS Photonics 2021, 8, 721.

[22]. Kuznetsov AI, Miroshnichenko AE, Brongersma ML, Kivshar YS, Luk'yanchuk B, Science 2016, 354.

[23]. Jahani S, Jacob Z, Nat. Nanotechnol 2016, 11, 23. [PubMed: 26740041]

[24]. Staude I, Schilling J, Nat. Photonics 2017, 11, 274.

[25]. Green TD, Baranov DG, Munkhbat B, Verre R, Shegai T, Käll M, Optica 2020, 7, 680.

[26]. Verre R, Baranov DG, Munkhbat B, Cuadra J, Kall M, Shegai T, Nat. Nanotechnol 2019, 14, 679. [PubMed: 31061517]

[27]. Munkhbat B, Baranov DG, Stührenberg M, Wersäll M, Bisht A, Shegai T, ACS Photonics 2019, 6, 139.

[28]. Zhang X, De-Eknamkul C, Gu J, Boehmke AL, Menon VM, Khurgin J, Cubukcu E, Nat. Nanotechnol 2019, 14, 844. [PubMed: 31406361]

[29]. Zhang H, Abhiraman B, Zhang Q, Miao J, Jo K, Roccasecca S, Knight MW, Davoyan AR, Jariwala D, Nat. Commun 2020, 11, 3552. [PubMed: 32669550]

[30]. Huang Y, Yu K, Li H, Xu K, Liang Z, Walker D, Ferreira P, Fischer P, Fan D, Adv. Mater 2020, 32, 2003439.

[31]. Abujetas DR, Paniagua-Domínguez R, Sánchez-Gil JA, ACS Photonics 2015, 2, 921.

[32]. Zengin G, Johansson G, Johansson P, Antosiewicz TJ, Käll M, Shegai T, Sci. Rep 2013, 3, 3074. [PubMed: 24166360]

[33]. Cao L, White JS, Park J-S, Schuller JA, Clemens BM, Brongersma ML, Nat. Mater 2009, 8, 643. [PubMed: 19578337]

[34]. Li S-Q, Crozier KB, Phys. Rev. B 2018, 97, 245423.

[35]. Cuadra J, Baranov DG, Wersall M, Verre R, Antosiewicz TJ, Shegai T, Nano Lett 2018, 18, 1777. [PubMed: 29369640]

[36]. Bisht A, Cuadra J, Wersall M, Canales A, Antosiewicz TJ, Shegai T, Nano Lett 2019, 19, 189. [PubMed: 30500202]

[37]. Munkhbat B, Baranov DG, Bisht A, Hoque MA, Karpiak B, Dash SP, Shegai T, ACS Nano 2020, 14, 1196. [PubMed: 31904217]

[38]. Zhang L, Gogna R, Burg W, Tutuc E, Deng H, Nat. Commun 2018, 9, 713. [PubMed: 29459736]

[39]. van de Groep J, Song J-H, Celano U, Li Q, Kik PG, Brongersma ML, Nat. Photonics 2020, 14, 426.

[40]. Choi W, Cho MY, Konar A, Lee JH, Cha G-B, Hong SC, Kim S, Kim J, Jena D, Joo J, Kim S, Adv. Mater 2012, 24, 5832. [PubMed: 22903762]

[41]. O'Donnell KP, Chen X, Appl. Phys. Lett 1991, 58, 2924.

[42]. Moody G, Kavir Dass C, Hao K, Chen C-H, Li L-J, Singh A, Tran K, Clark G, Xu X, Berghäuser G, Malic E, Knorr A, Li X, Nat. Commun 2015, 6, 8315. [PubMed: 26382305]

[43]. Lo TW, Zhang Q, Qiu M, Guo X, Meng Y, Zhu Y, Xiao JJ, Jin W, Leung CW, Lei D, ACS Photonics 2019, 6, 411.

[44]. Duh Y-S, Nagasaki Y, Tang Y-L, Wu P-H, Cheng H-Y, Yen T-H, Ding H-X, Nishida K, Hotta I, Yang J-H, Lo Y-P, Chen K-P, Fujita K, Chang C-W, Lin K-H, Takahara J, Chu S-W, Nat. Commun 2020, 11, 4101. [PubMed: 32796839]

[45]. Fang J, Wang M, Yao K, Zhang T, Krasnok A, Jiang T, Choi J, Kahn E, Korgel BA, Terrones M, Li X, Alù A, Zheng Y, Adv. Mater 2021, 33, 2007236.

[46]. Hu G, Hong X, Wang K, Wu J, Xu H-X, Zhao W, Liu W, Zhang S, Garcia-Vidal F, Wang B, Lu P, Qiu C-W, Nat. Photonics 2019, 13, 467.

[47]. Hong X, Hu G, Zhao W, Wang K, Sun S, Zhu R, Wu J, Liu W, Loh KP, Wee ATS, Wang B, Alù A, Qiu C-W, Lu P, Research 2020, 2020, 9085782. [PubMed: 32328579]

[48]. Ding L, Morits D, Bakker R, Li S, Eschimese D, Zhu S, Yu YF, Paniagua-Dominguez R, Kuznetsov AI, ACS Photonics 2020, 7, 1001.

[49]. Iyer PP, DeCrescent RA, Lewi T, Antonellis N, Schuller JA, Physical Review Applied 2018, 10, 044029.

[50]. Li J, Liu Y, Lin L, Wang M, Jiang T, Guo J, Ding H, Kollipara PS, Inoue Y, Fan D, Korgel BA, Zheng Y, Nat. Commun 2019, 10, 5672. [PubMed: 31831746]

[51]. Li J, Zheng Y, Acc. Mater. Res 2021, 2, 352. [PubMed: 34396151]

[52]. Kim K, Xu X, Guo J, Fan DL, Nat. Commun 2014, 5, 3632. [PubMed: 24709694]

[53]. Fan DL, Zhu FQ, Cammarata RC, Chien CL, Nano Today 2011, 6, 339.

[54]. Li Y, Chernikov A, Zhang X, Rigosi A, Hill HM, van der Zande AM, Chenet DA, Shih E-M, Hone J, Heinz TF, Phys. Rev. B 2014, 90, 205422.

[55]. Beal AR, Hughes HP, J. Phys. C: Solid State Phys 1979, 12, 881.

[56]. Gu X, Li B, Yang R, J. Appl. Phys 2016, 119, 085106.

[57]. Bernardi M, Palummo M, Grossman JC, Nano Lett 2013, 13, 3664. [PubMed: 23750910]

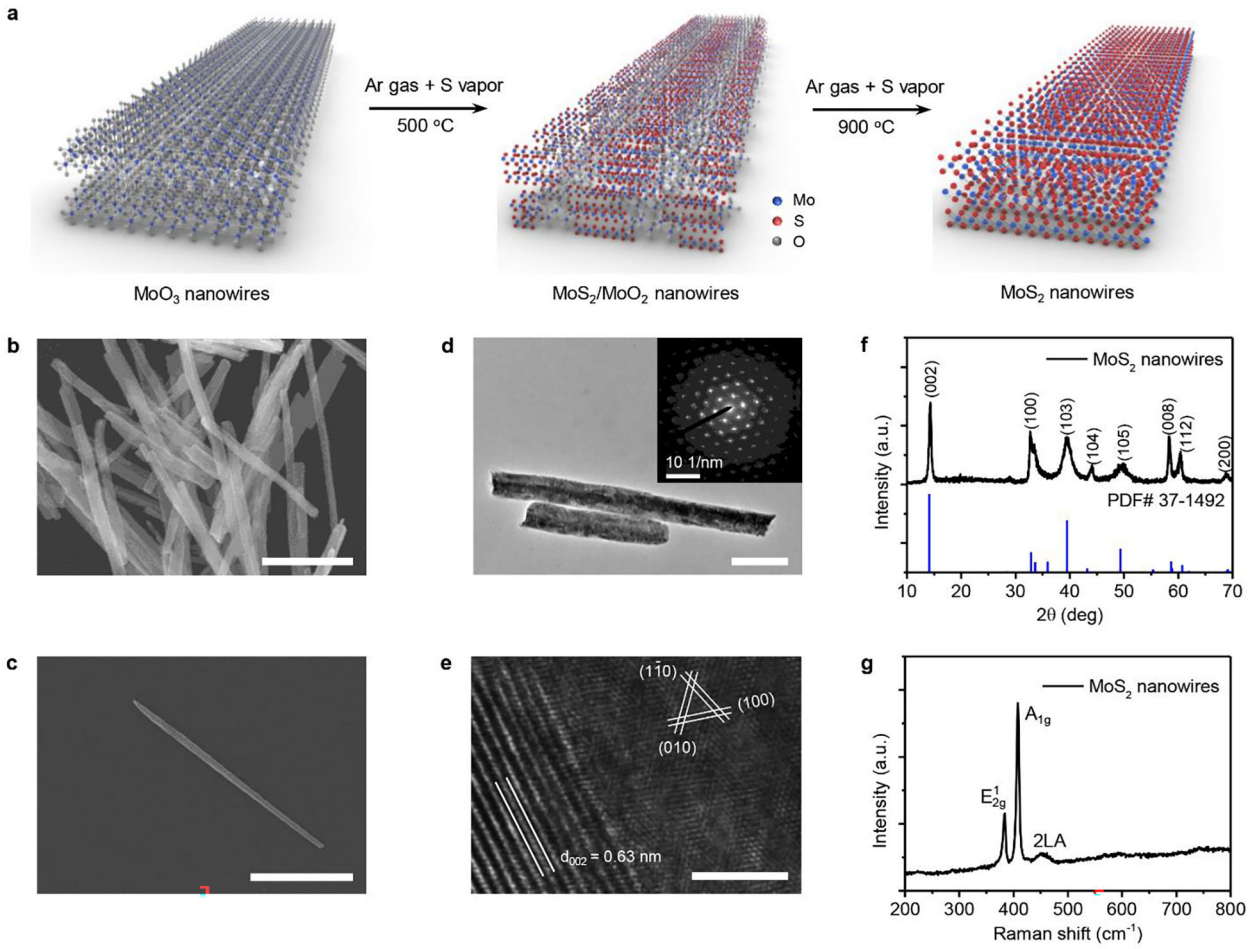

Figure1.

Colloidal MoS_2 nanowires. a) Schematic showing the synthesis of MoS_2 nanowires from MoO_3 nanowire precursors. b,c) SEM images of the as-synthesized MoS_2 nanowires. d,e) Phase-contrast TEM images of MoS_2 nanowires. The inset in (d) shows the SEAD pattern. f,g) The corresponding (f) XRD and (g) Raman spectra of MoS_2 nanowires. Scale bars: (b) 3 μm, (c) 5 μm, (d) 500 nm, (e) 5 nm.

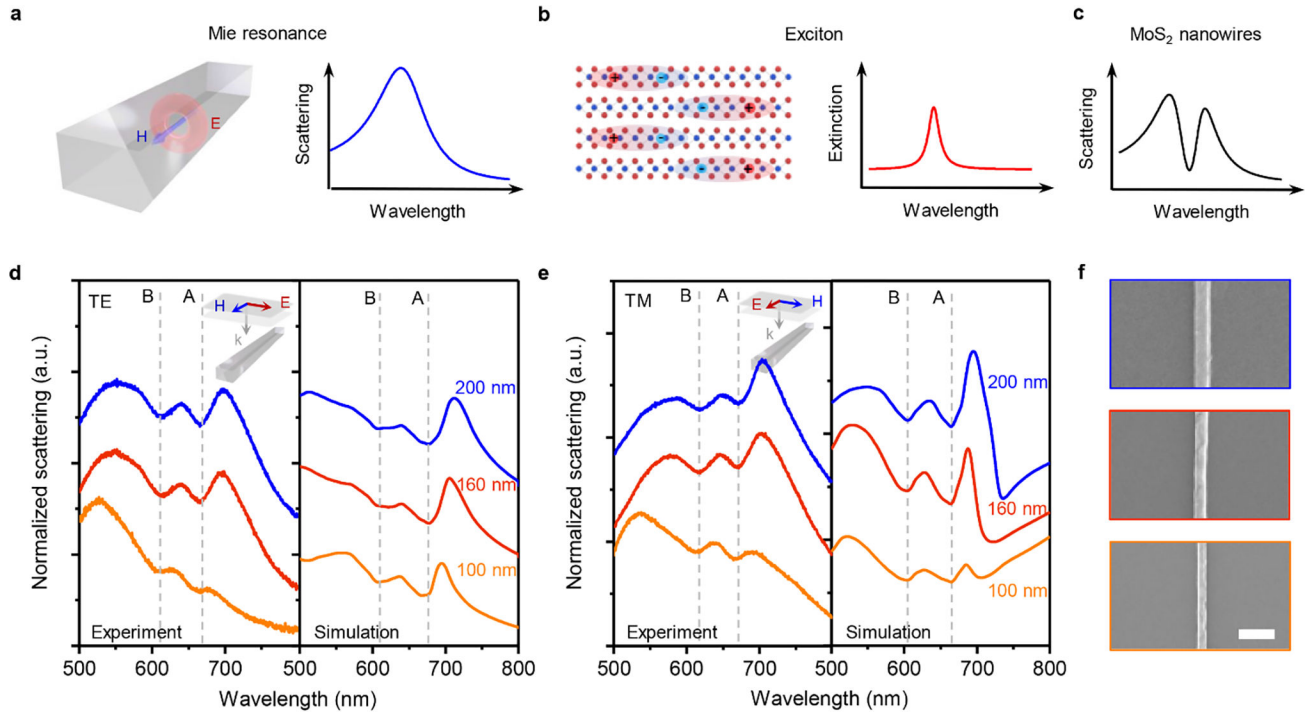

Figure 2.

Optical scattering response of individual MoS_2 nanowires. a-c) Schematic illustration showing the optical properties and scattering responses of TMDC nanowires: (a) Mie resonance, (b) exciton resonance, and (c) total scattering with the coupling between exciton and Mie resonances. d,e) Optical scattering spectra of MoS_2 nanowires with a width of 100, 160, and 200 nm under (d) TE- and (e) TM-polarized plane wave excitation (Insets show the schematics of the corresponding experimental geometries). f) Corresponding SEM images of the measured MoS_2 nanowires in (d) and (e). Scale bar: 500 nm.

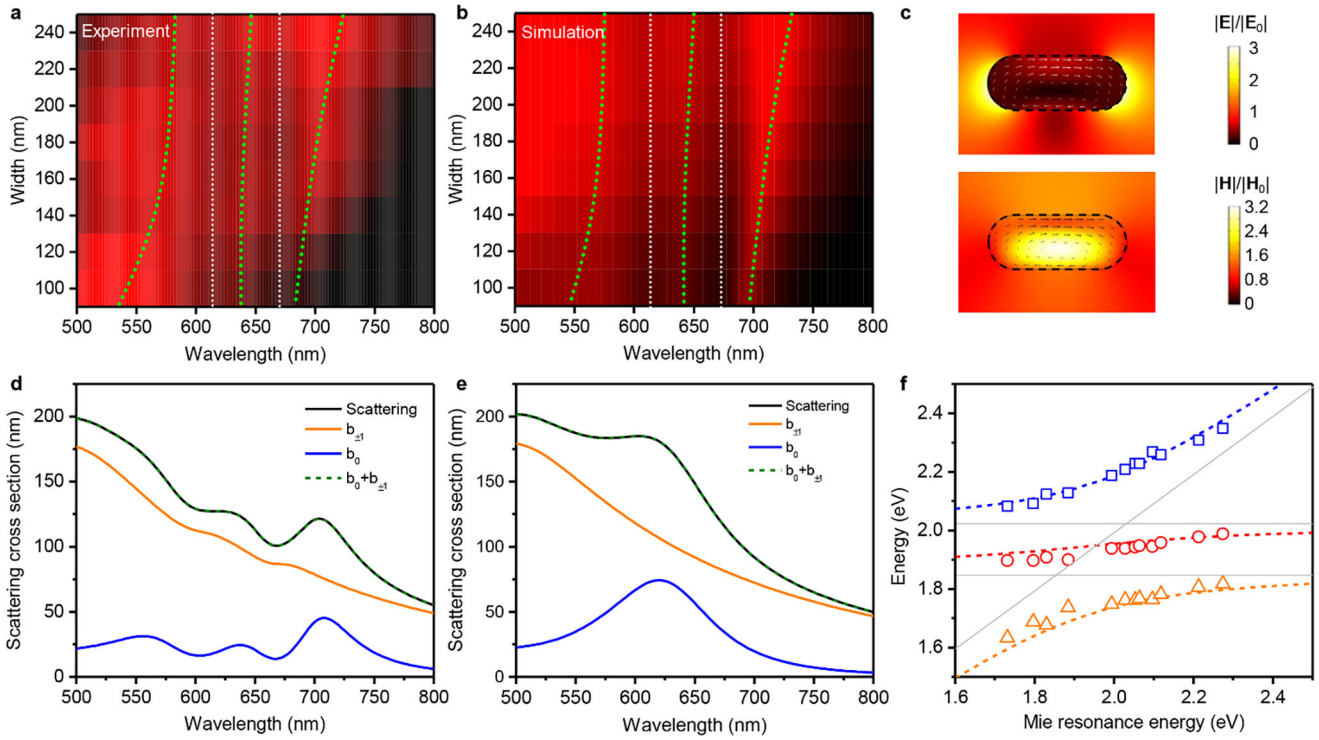

Figure 3.

Strong coupling in individual MoS_2 nanowires under TE-polarized excitation. a) Experimental normalized dark-field scattering map for MoS_2 nanowires with a thickness of 65 nm and a varying width from 100 to 240 nm. b) The corresponding simulated scattering map of (a). The green dot lines depict three polariton branches. The grey dot lines show the positions of A and B excitons. c) Simulated electric and magnetic field intensity in the cross-section of a MoS_2 nanowire with a width of 160 nm at the wavelength of 640 nm, revealing the typical patterns of a magnetic dipole resonance. Arrows denote the electric field vectors inside the nanowire. d) Simulated scattering cross section (black solid curve) of a MoS_2 nanowire with a width of 150 nm in vacuum. Also shown are the contributions to total scattering by decomposed magnetic dipole mode (b_0, blue curve), electric dipole mode ($b_{\pm1}$, orange curve), and their sum (green dashed curve). e) Same as (d), except that the oscillator strengths of A and B excitons are set to 0 in the dielectric function. f) Anticrossing behaviors of three polariton branches. Colored dots represent experimental polariton eigen energies as a function of Mie resonance energy; colored dashed lines depict the eigen energies obtained from Hamiltonian analysis; and grey solid lines indicate the exciton (horizontal lines) and Mie (diagonal line) resonances.

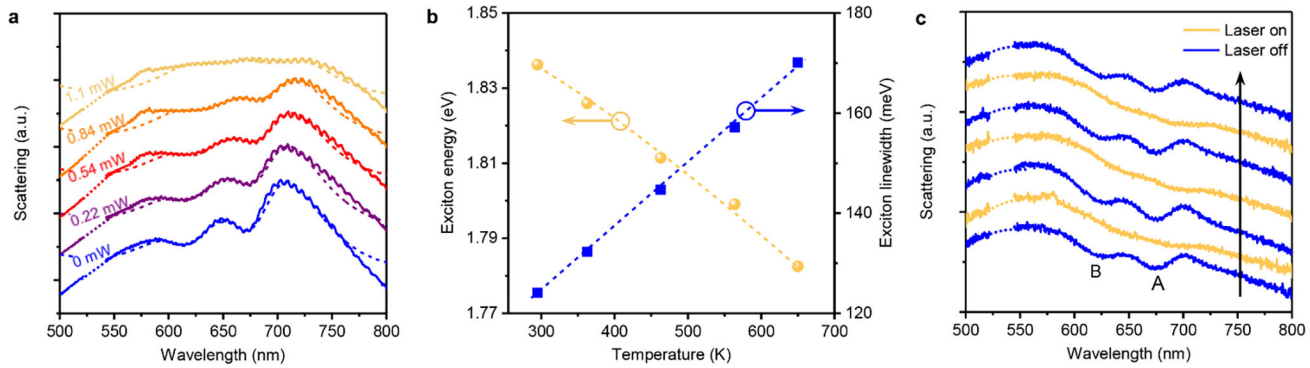

Figure 4.

Optical modulation of excitons. a) Measured scattering spectra of a MoS_2 nanowire under 532 nm laser irradiation with an optical power of 0, 0.22, 0.54, 0.84, and 1.1 mW. The dashed lines show the CMT fitting curves. b) Temperature-dependent energy and linewidth of A exciton. The yellow and blue dashed lines show the corresponding fitting curves by the O'Donnell model and linear fitting, respectively. c) High reproducibility of the cycling (along the black arrow) of optical scattering spectra between laser on and off states.

Table 1.

Parameters used in the Hamilton analysis.

g_A (meV)	g_B (meV)	γ_A (meV)	γ_B (meV)	γ_{MD} (meV)
160	140	120	160	310